Characterisation of Chip Morphology in Orthogonal Cutting of Medical Grade Cobalt Chromium Alloy (ASTM F1537)

S.Baron[1] and E.Ahearne[1]

1. University College Dublin, School of Mechanical and Materials Engineering.

ABSTRACT

Cobalt Chromium alloys (CoCr) are used in the manufacture of class 3 medical devices, notably knee and hip implants, due to singular mechanical properties such as wear resistance and biocompatibility. Notwithstanding the importance of the material, there has been limited research reported on the fundamental mechanism in machining of this alloy. This paper initially propounds on the properties that define a material as "difficult to cut" (DTC) in order to compare machining related properties of ASTM F1537 CoCr with other known DTC alloys. This is followed by a brief summary of literature specifically on the chip morphology produced in turning of ASTM F136 Ti-6Al-4V and Inconel 718. Orthogonal cutting tests are then undertaken to examine the chip morphology in cutting ASTM F1537 over a range of cutting speeds (V_c) and levels of undeformed chip thickness (h_m). The findings of this research were compared with those found in literature. It is concluded that ASTM F1537 CoCr produced segmented chips under all tested conditions and chip segmentation frequency increases with the cutting speed but is independent of the undeformed chip thickness. Moreover, the ratio of the segment height to the maximum chip thickness was found to decrease with cutting speed.

Keywords: Cobalt Chromium, Orthogonal Cutting, Chip Morphology.

UNITS AND ACRONYMS:

V_c – Cutting Speed	[m/min]	h_m – Uncut Chip Thickness	[µm]
w – Width of cut	[mm]	ϕ- Rake Angle	[°]
L_c – Chip length.	[µm]	σ – Standard deviation.	[n/a]
f_c- Segmentation Freq.	[kHz]	h_c –Max. chip thickness.	[µm]
h_s Segment Height	[µm]		

INTRODUCTION:

Cobalt chromium alloys, are widely used for orthopaedic implants. These components require optimum stiffness, excellent biocompatibility and good wear resistance of tribological polished surfaces. Figure 1 shows DePuy's "Attune Fixed Bearing" implant, where both femoral component and Tibial tray are made from ASTM F75 CoCr.

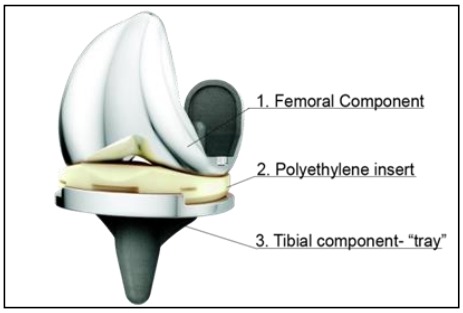

Figure 1: Attune Fixed bearing knee assembly.

Cobalt Chromium alloys were initially developed in 1907 [1] but ongoing research and development has improved the available range of mechanical properties due to improvements in composition and processing, including post casting treatment [4]. The cobalt (Co) base metal nominally forms a HCP structure which contributes to its required mechanical properties while alloying with Chromium (Cr) improves corrosion resistance [2]. Corrosion resistance is attributed to the formation of a hard passive oxide layer [3]. A metastable FCC phase dominates in as cast ASTM F75 alloy at room temperature. Due to this structure, CoCrMo alloys are characterised with high strength- strain hardening rates and ability to absorb stresses by a FCC to HCP transformation [4]. CoCr alloys have a two phase dendritic solidification process. Dendritic regions are nobler (etch with more difficulty), rich in cobalt ($\gamma - phase$) and have a FCC structure. The interdendritic regions are a less noble phase characterised by a HCP structure [5]. Figure 2 shows a phase diagram of the binary CoCr alloy based on a theoretical modelling approach [6].

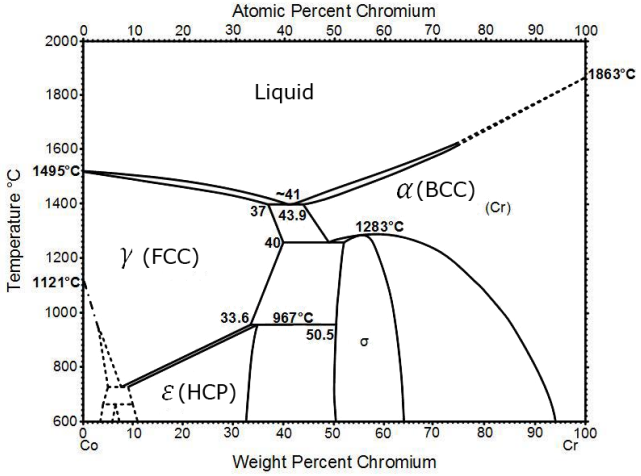

Figure 2: Phase diagram of binary CoCr alloy [7].

Carbon content causes the formation of hard carbides which disperse in alloyed matrix and precipitate at grain boundaries. Careful adjustment of carbon content,

carbide dispersion and precipitation is essential to achieve optimum mechanical properties. Alloying with Molybdenum causes the formation of new hard carbides which (a) disperse in alloyed matrix, increasing the strength of the alloy and (b) precipitate at grain boundaries supressing gross sliding and dislocation migration. The mechanical properties of CoCr can be further refined by post casting treatment, for example, age hardening promotes FCC to HCP transformation [8]. Nickel is a common sensitizer found in human body, therefore can cause allergic reaction, so its content in implantable devices should be kept to a minimum. However, alloying with Ni alters the solidification process, (only 11Co-8Cr-Ni and 6Co-3Cr-Ni have dendritic solidification) and promotes stabilization of y (FCC) phase [9]. While ASTM F75 and ASTM F1537 limit the nickel content to <0.1%, in order to improve plasticity, ASTM F90 and ASTM F552 alloys contain higher nickel content.

Shaw states that machinability of a material is a function of its chemistry, structure and compatibility with work material. Titanium alloys are generally considered to be difficult to cut because of [10]:

1) Low thermal conductivity and specific heat, which causes high cutting temperatures.
2) The strong tendency for chips to weld and cause attritious wear.
3) Low strain in the chip leading to a high shear angle and small contact length between the chip and the tool.
4) Low value of Young's modulus.

While machinability of Nickel and cobalt base materials is hindered by [10]:

1) Tendency for maximum tool-face temperature to be close to the tool tip.
2) High work hardening rates leading to high machining forces.
3) Tendency to form a "build up edge (BUE)".
4) Low thermal conductivity leading to high temperatures.

On that basis, key physical and mechanical properties of difficult to cut materials considered in this work are:

(a) Flow stress (σ_y) which is a function of strain, strain rate, and temperature. It primarily determines cutting forces exerted on the tool.
(b) Thermal diffusivity which determines how effectively a given material can dissipate generated heat. Thermal diffusivity is related to thermal conductivity, density and specific heat capacity.
(c) Friction or shear stress at tool-work piece interface which depends on the nature of the friction mechanisms (adhesion, abrasion, physio-chemical reactions etc.) and the global-local application-specific process parameters, such as coolant application strategy which affect these mechanisms [10].

Table 1 summarises machinability related parameters of biomedical ASTM F1537, ASTM F136 Ti-6Al-4V and Inconel 718. It is evident that ASTM F1537 CoCr, when compared to ASTM F136 is characterised by higher strength, higher hardness, and higher thermal diffusivity. It is important to note that the listed properties compare these alloys at room temperature in the absence of full constitutive relationships for CoCr.

	Units	ASTM 1537 CoCr	ASTM F136 Ti-6Al- 4V	Inconel 718
Proof Stress (0.2%)	MPa	928	870	1,035
Tensile Strength	MPa	1403	940	1,240
Elongation (Z)	%	29	16	25
Young's Modulus	GPa	283	114	204
Density	$Kg.m^{-3}$	8,768	4,420	8,190
Thermal Conductivity	$W.m^{-1}.K^{-1}$	14.8	7.2	11.2
Specific Heat Capacity	$J.Kg^{-1}.K^{-1}$	452	560	435
Thermal Diffusivity	$m^2.s^{-1}$	3.73E-06	2.91E-06	3.14E-06
Hardness	HRC	40	31	36

Table 1: Properties of DTC materials for room temp .

Chips are a by-product of mechanical machining. Examination of the morphology can elucidate mechanisms at the tool-workpiece interface [10]. It is well established that at cutting speeds above 60 m/min Ti-6Al-4V forms characteristic shear localised (saw tooth) chip. This is attributed to "adiabatic shearing" which relies on shear instability- formation of the narrow shear band. In case of Titanium this is due to material softening [11].
The alternative crack initiation theory assumes the formation of a crack originating at the free surface of the workpiece which propagates towards tool tip. Regardless of the mechanism of formation, chip segmentation affects cutting forces exerted on the cutting tool as illustrated in Figure 3 [10], [12]

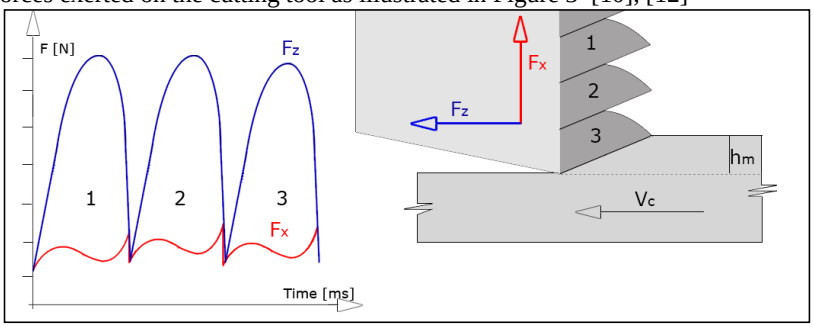

Figure 3: Segmented chip formation and cutting forces for 0°rake angle [10].

Variation in F_f and F_z due to chip segmentation occurs at relatively high frequencies and can have a significant effect on chatter stability [13]. Finally, the segmented chip formation may be correlated with tool wear [14].
Table 2 outlines the chip characteristics produced in machining of ASTM F136 and Inconel 718 for a range of cutting conditions [15].

References:	Material:	Cutting Conditions:	Conclusions on Chip Morphology:
[16]	Inconel 718	Dry Turning. V_c 30 - 50 [m/min] h_m 80 – 240 [μm]	Saw tooth chip due to cyclic crack formation. Segmentation frequency correlated with cutting force fluctuation.
[17]	Inconel 718	Turning, Used 10% water soluble coolant. V_c150-300[m/min] h_m 200[μm]	Higher cutting speed resulted in accelerated insert wear. Segmented chip observed.
[18]	Inconel 718	Orthogonal Turning V_c 10 – 213[μm]	Segmented chip formation above 61 m/min due to localised due to material softening.
[19]	Ti-6Al-4V	Dry, Orthogonal Turning V_c 4 – 120 [m/min] h_m 50, 70, 100 [μm]	Saw tooth chip due to adiabatic shear band. Chip segmentation increased with V_c.
[15]	Ti-6Al-4V	Dry, Orthogonal Turning. V_c 4 – 120 [m/min] h_m 50, 70, 100 [μm]	Saw tooth chip. Segment shear angle increased with V_c.
[20]	Ti-6Al-4V	Quick Stop. V_c 300 - 6000 [m/min] h_m 35 – 70 [μm]	Saw tooth chip- cyclic crack formation & adiabatic shear band.

Table 2: Summary of literature review into chip morphology of DTC materials.

EXPERIMENTAL METHOD:

In order to examine the chip morphology over a range of cutting conditions, a full factorial, orthogonal cutting experiment was performed. Morphology examination included measurement of geometrical characteristics, namely: segment length- L_c, maximum chip thickness- h_c and segment height- h_s. A 3mm wide disc was turned down on a HAAS TL2 CNC Lathe. The test order was randomised and every second cut was repeated; a new cutting edge was used for every test.. The experimental parameters were selected based on the literature review In order to ensure maximum tool and workpiece stability, a custom designed dynamometer and tool holders were deployed. The test parameters are presented in Table 3 and the experimental setup is presented in Figure 4. After each cut, the generated chips were collected, stored and labelled. The machine was then carefully cleaned from any remaining swarf. Collected chips were hot mounted in an epoxy resin, ground and polished. Subsequent microscopic examination allowed for the measurement of the chip geometry.

The median values of average segment length- L_c, maximum chip thickness- h_c, and segment height h_s (See Figure 5) were evaluated from 5 unique chip segments. This allowed for the evaluation of segmentation frequency: defined as formation of chip segments per unit time as expressed in equation 1.

$$f_c = \frac{V_c \sin\phi}{L_c} \qquad (1)$$

CUTTING CONDITIONS:				
CUTTING SPEED [m/min]	23	36	48	70
UNDEFORMED CHIP THICKNESS: [µm]		15	30	45
RAKE ANGLE: [°]		0		
RELIEF ANGLE: [°]		7		
CUTTING EDGE RADIUS: [µm]		14		
INSERT TYPE:		SCMW 120408 H13A		
COOLANT TYPE:		FUSCH ECOCOOL ULTRALIFE A		
COOLANT FLOW: [l/min]		2.5		
COOLANT CONCENTRATION [%]		8.50		

Table 3: Experimental parameters & cutting parameters.

RESULTS & DISCUSSION:

The focus of this experiment was on the influence of the cutting conditions, V_c and h_m, on chip morphology namely (see Figure 5):

a) Chip segmentation frequency: f_c
b) Maximum chip thickness: h_c
c) Segment height: h_s

The formation of a shear localised "saw tooth" chip was observed in each test. In order to fully determine the mechanism of chip segmentation, further tests are required. Initial inspection may suggest that the mechanism of saw tooth chip formation is due to crack initiation at the free surface.

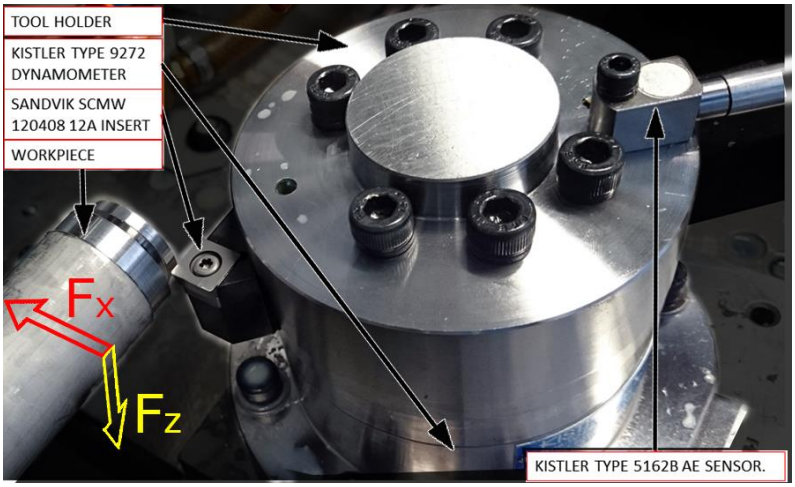

Figure 4: Orthogonal turning setup displaying dynamometer, tool, tool holder and the workpiece.

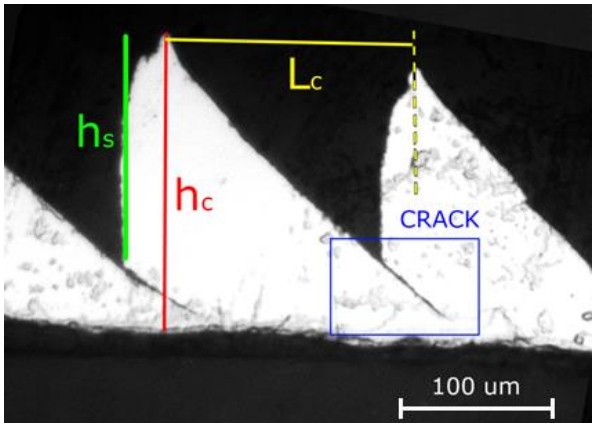

Figure 5: ASTM F1537 CoCr Chip morphology formed at V_c=48 h_m=15.

f_c segmentation frequency [kHz]		h_m [um]			h_c max.chip thickness [um]		h_m [um]		
		15	30	45			15	30	45
V_c [m/min]	25	9.0	7.6	3.3	V_c [m/min]	25	52	57	136
	36	13.3	7.2	5.2		36	51	88	135
	48	19.3	14.7	7.0		48	44	54	128
	70	31.3	24.9	14.1		70	42	104	154

Table 4: Presents computed results of chip morphology analysis- segmentation frequency and segment height

Within the test envelope, the segmentation frequency was found to increase with V_c and decrease for higher h_m. This is shown in Figure 6. It was also found that segment spacing decreases with increasing cutting speed. Segmentation frequency is therefore also reflected in the chip geometry.

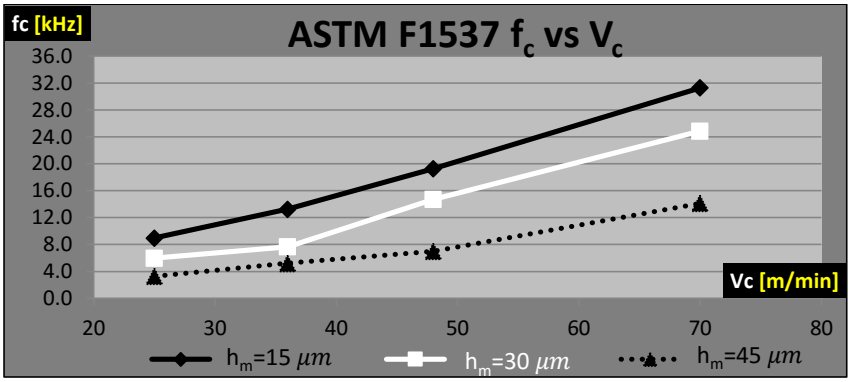

Figure 6: ASTM F1537 CoCr Segmentation Frequency vs. Cutting Speed.

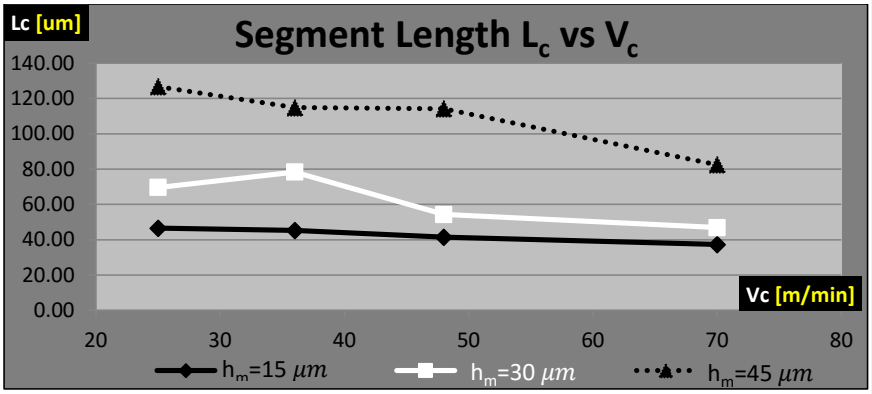

Figure 7: ASTM F1537 CoCr Segment Length vs. Cutting Speed.

The maximum chip thickness was found to increase with h_m, and remained relatively independent of V_c,as shown in Figure 8.

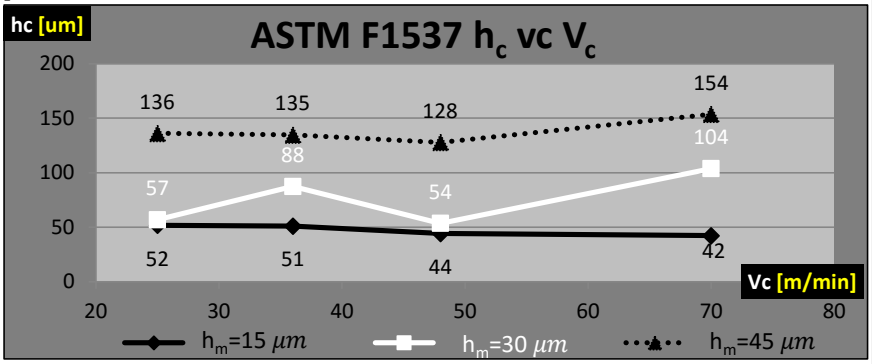

Figure 8: ASTM F1537 CoCr Segment height vs. Cutting Speed.

An analysis of the segmentation ratio, defined as h_s/h_c , revealed that it decreases for higher cutting speed and increases with depth of cut, as shown in Figure 9.

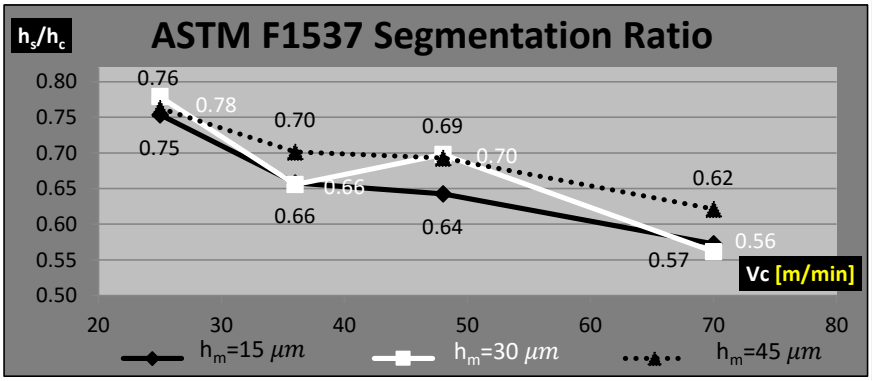

Figure 9: Chip segmentation ratio as a function of cutting speed.

It may be concluded therefore that:

1) An increase of undeformed chip thickness resulted in a decrease of segmentation frequency and a higher segmentation ratio.

2) An increase of cutting speed resulted in lower segment length, higher segmentation frequency and a lower segmentation ratio. (See Figure 10)

Microscopic examination of the chip morphology has shown a crack propagating from the free surface towards the tool tip. This crack ceases near secondary shear zone, as shown on Figure 5. This may suggest that theory of crack initiation at the free surface could be the fundamental mechanism of CoCr chip segmentation. In such a case, a reported decrease of segment height at higher cutting speed may be explained by presence of thicker secondary shear zone at higher cutting speeds. Due to thermal softening of the material crack propagation is hindered.
It is also expected that the examination of the cutting forces will reveal a cutting force fluctuation at the segmentation frequency with a force fluctuation that is proportional to the segmentation ratio. This is a topic for future work.

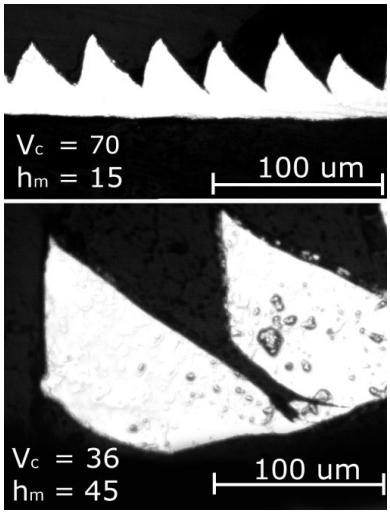

Figure 10 Chip Morphology for two different cutting conditions.

FUTURE WORK:

Future work will examine the cutting force components monitored over a range of main cutting parameters to evaluate the Kienzle equation coefficients for ASTM F1537 and ASTM F75.This will be followed by modelling and model verification for milling using ESPRIT CAD/CAM software.
Higher segmentation ratio is also expected to correlate with high fluctuation of cutting forces. This will be examined and reported in follow up work.

Formatted: IMC 32 Body

ACKNOWLEDGEMENTS:

We would like to thank DePuy Synthes and Enterprise Ireland for supporting this research through the Innovation Partnership (IP) programme. The Innovation Partnership programme is co-funded by the European Union through the European Regional Development Fund 2014-2020.

We would also like to thank the Machine Tool Technologies Research Foundation (MTTRF) and their sponsors, DMG Mori and DP Technologies (Esprit), for providing the facilities used in the course of this project.

Formatted: Font: (Defaul color: Auto

Formatted: IMC 32 Body

Formatted: Font: (Defaul color: Auto

REFERENCES:

1. Al Jabbari, Y.S., *Physico-mechanical properties and prosthodontic applications of Co-Cr dental alloys: a review of the literature.* The journal of advanced prosthodontics, 2014. **6**(2): p. 138-145.
2. Sikkenga, C. and C.A. Castings, *Casting, vol. 15.* ASM Handbook, ASM International, 2008: p. 1114-1118.
3. Ramsden, J.J., et al., *The Design and Manufacture of Biomedical Surfaces.* CIRP Annals - Manufacturing Technology, 2007. **56**(2): p. 687-711.
4. Bedolla-Gil, Y. and M. Hernandez-Rodriguez, *Tribological behavior of a heat-treated cobalt-based alloy.* Journal of materials engineering and performance, 2013. **22**(2): p. 541-547.
5. Montero-Ocampo, C., R. Juarez, and A.S. Rodriguez, *Effect of fcc-hcp phase transformation produced by isothermal aging on the corrosion resistance of a Co-27Cr-5Mo-0.05C alloy.* Metallurgical and Materials Transactions A, 2002. **33**(7): p. 2229-2235.
6. Matković, T., P. Matković, and J. Malina, *Effects of Ni and Mo on the microstructure and some other properties of Co–Cr dental alloys.* Journal of Alloys and Compounds, 2004. **366**(1–2): p. 293-297.
7. Ishida, K. and T. Nishizawa, *The Co-Cr (cobalt-chromium) system.* Bulletin of Alloy Phase Diagrams, 1990. **11**(4): p. 357-370.
8. Ramírez-Vidaurri, L.E., et al., *Cooling rate and carbon content effect on the fraction of secondary phases precipitate in as-cast microstructure of ASTM F75 alloy.* Journal of Materials Processing Technology, 2009. **209**(4): p. 1681-1687.
9. Mori, M., et al., *Microstructures and Mechanical Properties of Biomedical Co-29Cr-6Mo-0.14 N Alloys Processed by Hot Rolling.* Metallurgical and Materials Transactions A, 2012. **43**(9): p. 3108-3119.
10. Shaw, M.C., *Metal cutting principles*. Vol. 2. 2005: Oxford university press New York.
11. Molinari, A., C. Musquar, and G. Sutter, *Adiabatic shear banding in high speed machining of Ti–6Al–4V: experiments and modeling.* International Journal of Plasticity, 2002. **18**(4): p. 443-459.
12. Barry, J. and G. Byrne, *Chip Formation, Acoustic Emission and Surface White Layers in Hard Machining.* CIRP Annals - Manufacturing Technology, 2002. **51**(1): p. 65-70.
13. Taylor, C.M., S. Turner, and N.D. Sims, *Chatter, process damping, and chip segmentation in turning: A signal processing approach.* Journal of Sound and Vibration, 2010. **329**(23): p. 4922-4935.
14. Davies, M.A., Y. Chou, and C.J. Evans, *On Chip Morphology, Tool Wear and Cutting Mechanics in Finish Hard Turning.* CIRP Annals - Manufacturing Technology, 1996. **45**(1): p. 77-82.

15. Cotterell, M. and G. Byrne, *Characterisation of chip formation during orthogonal cutting of titanium alloy Ti–6Al–4V.* CIRP Journal of Manufacturing Science and Technology, 2008. **1**(2): p. 81-85.
16. Zhang, S., et al., *Saw-tooth chip formation and its effect on cutting force fluctuation in turning of Inconel 718.* International Journal of Precision Engineering and Manufacturing, 2013. **14**(6): p. 957-963.
17. Altin, A., M. Nalbant, and A. Taskesen, *The effects of cutting speed on tool wear and tool life when machining Inconel 718 with ceramic tools.* Materials & Design, 2007. **28**(9): p. 2518-2522.
18. Kaynak, Y., *Evaluation of machining performance in cryogenic machining of Inconel 718 and comparison with dry and MQL machining.* The International Journal of Advanced Manufacturing Technology, 2014. **72**(5-8): p. 919-933.
19. Cotterell, M. and G. Byrne, *Dynamics of chip formation during orthogonal cutting of titanium alloy Ti–6Al–4V.* CIRP Annals - Manufacturing Technology, 2008. **57**(1): p. 93-96.
20. Gente, A., H.W. Hoffmeister, and C.J. Evans, *Chip Formation in Machining Ti6Al4V at Extremely High Cutting Speeds.* CIRP Annals - Manufacturing Technology, 2001. **50**(1): p. 49-52.